11 Ultrasonic Measurement Models

In the previous Chapters we have shown that in order to predict the measured signals in an ultrasonic test one needs to know the system function, $s(\omega)$, and the acoustic/elastic transfer function, $t_A(\omega)$ of the system. Then the frequency components of the measured voltage, $V_R(\omega)$, are given by

$$V_R(\omega) = s(\omega) t_A(\omega). \tag{11.1}$$

We have seen how to obtain the system function, either by measurement of all the electrical and electromechanical components that it contains, or by a direct measurement in a calibration setup. In either case, if a flaw measurement is made with the same components and under the same conditions that the system function, $s(\omega)$, is measured, this same system function can be used in Eq. (11.1) for the flaw measurement. We have also given explicit expressions for the acoustic/elastic transfer function in some simple calibration setups. For a flaw measurement we need also to be able to describe this transfer function in terms of quantities that can be modeled or measured. Once such a transfer function is known, Eq. (11.1) provides a complete *ultrasonic measurement model* of the flaw measurement system. This Chapter will describe how to construct models of the acoustic/ elastic transfer function and the types of overall measurement models that result.

11.1 Reciprocity-based Measurement Model

It will be shown in this section that the acoustic/elastic transfer function can be modeled with reciprocity relations for fluid and elastic media. These reciprocity relations are very general, relying primarily on the assumption of linearity of the media involved. We have already seen reciprocity play a role in defining the electrical and electromechanical components of a measurement system. For purely electrical components, like the cable, reciprocity was given in terms of the electrical input and

output voltages and currents of a two port system in the form (see Eq. (3.3)):

$$V_1^{(1)} I_1^{(2)} - V_1^{(2)} I_1^{(1)} = V_2^{(1)} I_2^{(2)} - V_2^{(2)} I_2^{(1)}. \tag{11.2}$$

Similarly the transducer satisfied a reciprocity relation between electrical and mechanical quantities (see Eq. (4.4)):

$$V^{(1)} I^{(2)} - V^{(2)} I^{(1)} = F^{(1)} v^{(2)} - F^{(2)} v^{(1)}. \tag{11.3}$$

To model the wave propagation and scattering processes contained in the acoustic/elastic transfer function, one needs to state similar reciprocity relations for the 3-D acoustic and elastic fields involved. For a fluid, for example, if one has a volume, V, of a fluid and two different wave fields (identified as states (1) and (2)) in that volume that satisfy the same homogeneous wave equation (no body force sources), then on the closed surface, S, of V we must have satisfied the reciprocity relationship [Fundamentals]

$$\int_S \left(p^{(1)} \mathbf{v}^{(2)} - p^{(2)} \mathbf{v}^{(1)} \right) \cdot \mathbf{n} dS = 0, \tag{11.4}$$

where $p^{(1)}, \mathbf{v}^{(1)}$ are the pressure and velocity fields for state (1), $p^{(2)}, \mathbf{v}^{(2)}$ are the pressure and velocity fields for state (2), and $\mathbf{n}$ is a unit vector normal to S.

Similarly for a linear, elastic solid, one has a reciprocity relationship between two stress and velocity fields acting in the same volume, V, of the same elastic material. If those two fields both satisfy Navier's equations in V for no body force sources, then [Fundamentals]

$$\int_S \left(\mathbf{t}^{(1)} \cdot \mathbf{v}^{(2)} - \mathbf{t}^{(2)} \cdot \mathbf{v}^{(1)} \right) dS = 0, \tag{11.5}$$

where $\mathbf{t}^{(1)}, \mathbf{v}^{(1)}$ are the stress (traction) vector and velocity vector for state (1) and $\mathbf{t}^{(2)}, \mathbf{v}^{(2)}$ are the stress vector and velocity vector for state (2). The Cartesian components of the stress vector are given in terms of the Cartesian stresses, τ_{ij}, in the solid by

$$t_i = \tau_{ji} n_j, \qquad (i = 1,2,3) \tag{11.6}$$

where n_j are the components of the normal to the surface, S, surrounding the volume.

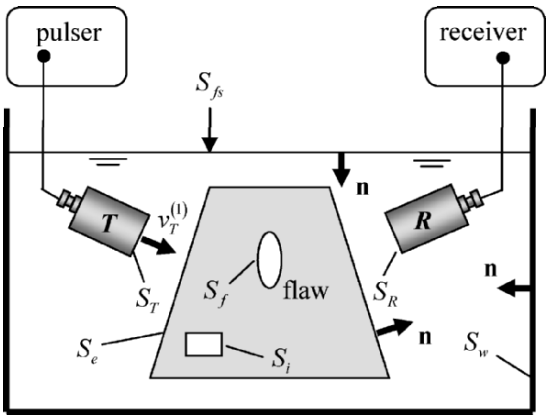

Fig. 11.1. An ultrasonic immersion flaw measurement system. This setup is designated as state (1) in our reciprocity relations.

We will demonstrate the application of these reciprocity relations to the flaw measurement system shown in Fig. 11.1. We will call this setup state (1). In this state we have the transmitting piston transducer, *T*, firing and generating a normal velocity, $v_T^{(1)}(\omega)$, on its surface, S_T, while the receiving transducer, *R*, is picking up the signals received from the flaw and other reflectors over its surface, S_R. The surface of the flaw itself is denoted as S_f. We have also labeled other surfaces in Fig. 11.1 as follows: Surface S_{fs} is the free surface of the fluid, S_w is the surface of the tank wall in contact with the fluid, S_e is the surface of the elastic solid being inspected, and S_i is the surface of one or more internal surfaces of the solid (other than the flaw). The unit normals to the various surfaces in contact with the fluid are also shown in Fig. 11.1. State (2) is shown in Fig. 11.2. In this state, we drive the "receiving" transducer R with a normal velocity, $v_R^{(2)}(\omega)$, on its surface, S_R, and we have the flaw in the component absent. We will also use a state (3), shown in Fig. 11.3. This state is identical to state (1), as shown in Fig. 11.3, except that the flaw is also absent in this state.

First, apply the reciprocity relationship to the common fluid region in states (1) and (2). There are no sources inside the fluid so we have:

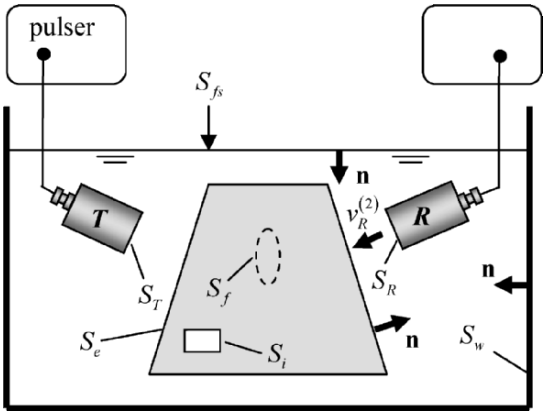

Fig. 11.2. The same measurement configuration as in Fig. 11.1 but where transducer R is assumed to be driven as a transmitter (the pulser driving T is quiescent) and the flaw is absent. The surface, S_f , is defined in this setup as the same surface that was occupied by the flaw in state (1). This configuration is designated as state (2) in the reciprocity relations.

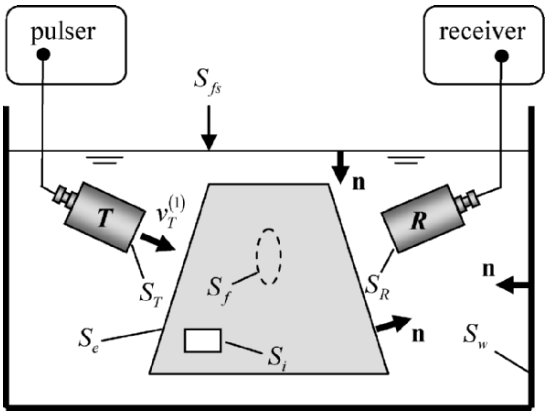

Fig. 11.3. The same configuration as shown in Fig. 11.1 except the flaw is now absent. The surface, S_f , is defined in this setup as the same surface that was occupied by the flaw in state (1). This configuration is designated as state (3) in the reciprocity relations.

$$\int_{S_{fs}+S_w+S_T+S_R+S_e+S_{other}} \left(p^{(1)}\mathbf{v}^{(2)} - p^{(2)}\mathbf{v}^{(1)} \right) \cdot \mathbf{n} dS = 0. \tag{11.7}$$

For both states (1) and (2) at the free surface we have $p^{(1)} = p^{(2)} = 0$ so that the integral over S_{fs} is zero and can be eliminated from Eq. (11.7). Similarly for the tank wall, which is assumed to be rigid, we have $\mathbf{v}^{(1)} \cdot \mathbf{n} = \mathbf{v}^{(2)} \cdot \mathbf{n} = 0$ so the integral over S_w can also be eliminated. The surface S_{other} includes all other surfaces in contact with the fluid not shown explicitly in Fig. 11.1. These other surfaces would be the surfaces of the cables, the parts of the transducer surfaces other than the active surfaces S_T and S_R and the surfaces of the supports (not shown) of the component being inspected. We will assume these other surfaces, like the tank wall, are rigid so they also can be eliminated from Eq. (11.7). [Note: strictly speaking, the assumption that the tank wall and other surfaces are rigid is not needed to eliminate them from Eq. (11.7). The integrals over those surfaces can be eliminated by simply using the fact that they do not themselves contain any acoustic sources.] These results then reduce Eq. (11.7) to the form

$$\int_{S_T+S_R} \left(p^{(1)}\mathbf{v}^{(2)} - p^{(2)}\mathbf{v}^{(1)} \right) \cdot \mathbf{n} dS = -\int_{S_e} \left(p^{(1)}\mathbf{v}^{(2)} - p^{(2)}\mathbf{v}^{(1)} \right) \cdot \mathbf{n} dS. \tag{11.8}$$

Since we have assumed the transducers are acting as pistons, we can remove the velocity terms from the integrals in Eq. (11.8), which leaves the remaining integrals of the pressure over the transducer faces as just force terms, and we obtain

$$\left(F_T^{(1)} v_T^{(2)} - F_T^{(2)} v_T^{(1)} \right) + \left(F_R^{(1)} v_R^{(2)} - F_R^{(2)} v_R^{(1)} \right) = -\int_{S_e} \left(p^{(1)}\mathbf{v}^{(2)} - p^{(2)}\mathbf{v}^{(1)} \right) \cdot \mathbf{n} dS \tag{11.9}$$

where $F_T^{(m)}, v_T^{(m)} \left(m = 1,2 \right)$ are the compressive forces and normal velocities at the surface, S_T, of the transmitting transducer in states (1) and (2), and $F_R^{(m)}, v_R^{(m)} \left(m = 1,2 \right)$ are the corresponding forces and normal velocities acting on the receiving transducer for those states. The directions of the normal velocities all are positive when pointing outwards from the transducer face into the fluid. On the surface, S_e, of the component being inspected the traction and normal velocity must be continuous, i.e. we have

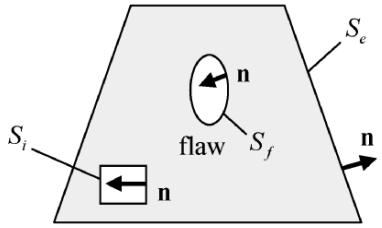

Fig. 11.4. The geometry of the solid component being inspected, showing the surfaces involved in the reciprocity relations and the directions of the unit normal on those surfaces.

$$\begin{aligned} -p^{(m)}\mathbf{n}\Big|_{fluid} &= \mathbf{t}^{(m)}\Big|_{solid} \\ \mathbf{v}^{(m)}\cdot\mathbf{n}\Big|_{fluid} &= \mathbf{v}^{(m)}\cdot\mathbf{n}\Big|_{solid} \end{aligned} \tag{11.10}$$

for m = 1,2 so that Eq. (11.9) can also be written in terms of the surface fields on the solid as

$$\begin{aligned} &\left(F_T^{(1)}v_T^{(2)} - F_T^{(2)}v_T^{(1)}\right) + \left(F_R^{(1)}v_R^{(2)} - F_R^{(2)}v_R^{(1)}\right) \\ &= \int_{S_e}\left(\mathbf{t}^{(1)}\cdot\mathbf{v}^{(2)} - \mathbf{t}^{(2)}\cdot\mathbf{v}^{(1)}\right)dS. \end{aligned} \tag{11.11}$$

Now, consider the volume of solid contained between the external surface, S_e, which is in contact with the fluid, and the internal surfaces consisting of the flaw surface, S_f, and other internal surfaces, S_i (Fig. 11.4). Since there are no sources of sound inside this volume, we must have

$$\int_{S_e+S_f+S_i}\left(\mathbf{t}^{(1)}\cdot\mathbf{v}^{(2)} - \mathbf{t}^{(2)}\cdot\mathbf{v}^{(1)}\right)dS = 0. \tag{11.12}$$

The surfaces S_i are present in both states (1) and (2). If those surfaces are traction free in both states (e.g. if there are holes in the component being inspected), or if those surfaces are source-free inclusions of other materials, the integral over S_i in Eq. (11.12) will vanish. We then find

$$\int_{S_e}\left(\mathbf{t}^{(1)}\cdot\mathbf{v}^{(2)} - \mathbf{t}^{(2)}\cdot\mathbf{v}^{(1)}\right)dS = -\int_{S_f}\left(\mathbf{t}^{(1)}\cdot\mathbf{v}^{(2)} - \mathbf{t}^{(2)}\cdot\mathbf{v}^{(1)}\right)dS \tag{11.13}$$

which, when placed into Eq. (11.11), gives

$$\begin{aligned}&\left(F_T^{(1)}v_T^{(2)} - F_T^{(2)}v_T^{(1)}\right) + \left(F_R^{(1)}v_R^{(2)} - F_R^{(2)}v_R^{(1)}\right)\\ &= -\int_{S_f}\left(\mathbf{t}^{(1)}\cdot\mathbf{v}^{(2)} - \mathbf{t}^{(2)}\cdot\mathbf{v}^{(1)}\right)dS.\end{aligned} \tag{11.14}$$

In Eq. (11.14), the unit normal to the flaw is directed inwards, as shown in Fig. 11.4. If we express the stress vector in terms of the stresses and let the components of this inward normal be n_j' Eq. (11.14) becomes

$$\begin{aligned}&\left(F_T^{(1)}v_T^{(2)} - F_T^{(2)}v_T^{(1)}\right) + \left(F_R^{(1)}v_R^{(2)} - F_R^{(2)}v_R^{(1)}\right)\\ &= -\int_{S_f}\left(\tau_{ji}^{(1)}v_i^{(2)} - \tau_{ji}^{(2)}v_i^{(1)}\right)n_j'dS.\end{aligned} \tag{11.15}$$

It is convenient, however, to switch the direction of the normal so that it points outwards from the flaw into the surrounding material. In that case, Eq. (11.15) becomes

$$\begin{aligned}&\left(F_T^{(1)}v_T^{(2)} - F_T^{(2)}v_T^{(1)}\right) + \left(F_R^{(1)}v_R^{(2)} - F_R^{(2)}v_R^{(1)}\right)\\ &= \int_{S_f}\left(\tau_{ji}^{(1)}v_i^{(2)} - \tau_{ji}^{(2)}v_i^{(1)}\right)n_j dS,\end{aligned} \tag{11.16}$$

where now n_j are the components of the *outward normal*.

We can follow exactly the same steps outlined here for states (1) and (2) but use states (3) and (2) instead. On the left hand side of Eq. (11.16) the force and velocity terms for state (1) will be replaced by those for state (3). The right hand side of equation (11.16) will be zero since the surface S_f is itself merely a fictitious surface surrounding a source free region in both states (2) and (3). Thus, we find

$$\left(F_T^{(3)}v_T^{(2)} - F_T^{(2)}v_T^{(3)}\right) + \left(F_R^{(3)}v_R^{(2)} - F_R^{(2)}v_R^{(3)}\right) = 0. \tag{11.17}$$

Now, we subtract Eq. (11.17) from Eq. (11.16) to obtain

$$\begin{aligned}&\left(\Delta F_T v_T^{(2)} - F_T^{(2)}\Delta v_T\right) + \left(\Delta F_R v_R^{(2)} - F_R^{(2)}\Delta v_R\right)\\ &= \int_{S_f}\left(\tau_{ji}^{(1)}v_i^{(2)} - \tau_{ji}^{(2)}v_i^{(1)}\right)n_j dS,\end{aligned} \tag{11.18}$$

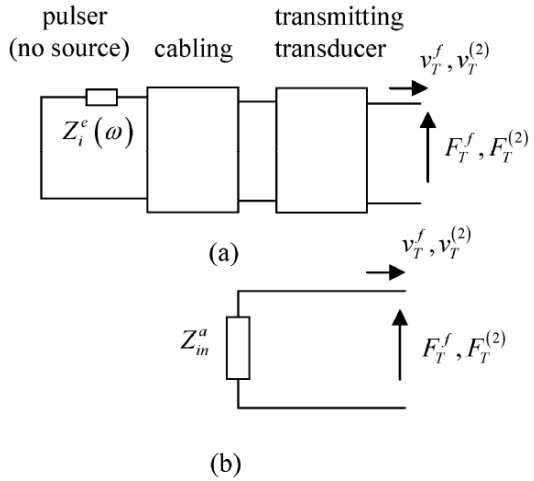

Fig. 11.5. (a) The force and velocity at the transmitting transducer due to the waves from the flaw or due to the waves in state (2), and **(b)** the corresponding equivalent acoustic impedance of the passive system shown in (a).

where

$$\begin{aligned}\Delta F_T &= F_T^{(1)} - F_T^{(3)} \\ \Delta v_T &= v_T^{(1)} - v_T^{(3)} \\ \Delta F_R &= F_R^{(1)} - F_R^{(3)} \\ \Delta v_R &= v_R^{(1)} - v_R^{(3)}.\end{aligned} \tag{11.19}$$

The quantities in state (1) appearing in Eq. (11.19) are due to all the waves received at either the transmitter or receiver from 1) either the flaw directly (or interactions that involve the flaw) and 2) with other interactions that do not involve the flaw at all. We will call the first type of contribution the flaw response and the second type of contribution the non-flaw response. The quantities in state (3) appearing in Eq. (11.19), however, come from exactly the same non-flaw response as in state (1). Thus, all the differences in Eq. (11.19) are only due to waves received from the flaw directly or due to interactions involving the flaw (such as a bounce of the incident wave from a surface to the flaw and then to the receiver). We will call these differences, therefore, the *flaw responses* and define them as

$$\begin{aligned} F_T^f &\equiv \Delta F_T \\ v_T^f &\equiv \Delta v_T \\ F_R^f &\equiv \Delta F_R \\ v_R^f &\equiv \Delta v_R . \end{aligned} \tag{11.20}$$

In terms of these flaw responses then Eq. (11.18) becomes

$$\begin{aligned} &\left(F_T^f v_T^{(2)} - F_T^{(2)} v_T^f\right) + \left(F_R^f v_R^{(2)} - F_R^{(2)} v_R^f\right) \\ &= \int_{S_f} \left(\tau_{ji}^{(1)} v_i^{(2)} - \tau_{ji}^{(2)} v_i^{(1)}\right) n_j dS \end{aligned} \tag{11.21}$$

Since the same incident, driving waves (and the same corresponding voltage sources) are present in both states (1) and (3), F_T^f is the force at the transmitting transducer due to waves coming from the flaw in the absence of any voltage sources at the transmitter. The same is true for $F_T^{(2)}$ since by definition the only voltage sources active in that state are driving the receiving transducer (see Fig. 11.5 (a)). Thus, as shown in Fig. 11.5 (b), for both the flaw force response at the transmitter *T* and for the force at *T* in state (2) one can replace the passive electrical and electromechanical components of the sound generation process by the same equivalent acoustic impedance, Z_{in}^a, where

$$\begin{aligned} F_T^f &= -Z_{in}^a v_T^f \\ F_T^{(2)} &= -Z_{in}^a v_T^{(2)} \end{aligned} \tag{11.22}$$

[the minus signs are due to the fact that the velocities appearing in Eq. (11.22) were both defined as the normal velocities directed outwards from the transducer, as shown in Fig. 11.5 (b)]. Placing Eq. (11.22) into Eq. (11.21), the terms at the transmitter all cancel, leaving

$$\left(F_R^f v_R^{(2)} - F_R^{(2)} v_R^f\right) = \int_{S_f} \left(\tau_{ji}^{(1)} v_i^{(2)} - \tau_{ji}^{(2)} v_i^{(1)}\right) n_j dS \tag{11.23}$$

In state (2), we have at the receiving transducer (which is firing as a transmitter) $F_R^{(2)} = Z_r^{R;a} v_R^{(2)}$, where $Z_r^{R;a}$ is the acoustic radiation impedance of the receiving transducer so Eq. (11.22) becomes:

$$\left(F_R^f - Z_r^{R;a} v_R^f\right) v_R^{(2)} = \int_{S_f} \left(\tau_{ji}^{(1)} v_i^{(2)} - \tau_{ji}^{(2)} v_i^{(1)}\right) n_j dS. \tag{11.24}$$

But the term in parentheses on the left side of Eq. (11.24) is just the total force at the receiver due to the waves from the flaw minus the force $F_s^f \equiv Z_r^{R;a} v_R^f$ due to the motion of the receiving transducer from the flaw response. By definition, this is just the blocked force, F_B, at the receiver due to the waves contained in the flaw response (see Eq. (5.24)), i.e.

$$F_B = F_R^f - Z_r^{R;a} v_R^f \tag{11.25}$$

and Eq. (11.24) can be rewritten as

$$F_B = \frac{1}{v_R^{(2)}} \int_{S_f} \left(\tau_{ji}^{(1)} v_i^{(2)} - \tau_{ji}^{(2)} v_i^{(1)}\right) n_j dS. \tag{11.26}$$

[Note that this blocked force is a force due only to wave interactions with the flaw, but we have dropped the superscript "f" and labeled the force simply F_B in order to be compatible with the notation used in previous Chapters.] Since the force at the transmitting transducer in our measurement setup is $F_t^{(1)} = Z_r^{T;a} v_T^{(1)}$, the acoustic/elastic transfer function, $t_A(\omega) = F_B / F_t^{(1)}$, for the measured flaw signals is given by

$$t_A(\omega) = \frac{1}{Z_r^{T;a} v_T^{(1)} v_R^{(2)}} \int_{S_f} \left(\tau_{ji}^{(1)} v_i^{(2)} - \tau_{ji}^{(2)} v_i^{(1)}\right) n_j dS. \tag{11.27}$$

When Eq. (11.27) is placed into Eq. (11.1), we have, finally a complete measurement model for the voltage received from the flaw, which can be written more explicitly as:

$$\begin{aligned} V_R(\omega) = & \frac{s(\omega)}{Z_r^{T;a} v_T^{(1)}(\omega) v_R^{(2)}(\omega)} \\ & \cdot \int_{S_f} \left[\tau_{ji}^{(1)}(\mathbf{x},\omega) v_i^{(2)}(\mathbf{x},\omega) - \tau_{ji}^{(2)}(\mathbf{x},\omega) v_i^{(1)}(\mathbf{x},\omega)\right] n_j(\mathbf{x}) dS, \end{aligned} \tag{11.28}$$

where $\mathbf{x}$ is a general point on the surface of the flaw and recall that the n_j are the components of the outward normal.

Equation (11.28) is a significant result. It shows that if we can measure the system function and model the stress and velocity fields present at the flaw in states (1) and (2), we can predict the measured voltage response of the flaw in virtually any flaw measurement system.

We obtained this result for the pitch-catch immersion setup of Fig. 11.1 but it can be equally applied to pulse-echo and contact testing setups as well. Since the fields in states (1) and (2) in Eq. (11.28) are divided by the driving normal velocities $v_T^{(1)}, v_R^{(2)}$ in states (1) and (2), we only need to model the fields in both states due to driving transducers having a unit normal velocity on their faces. Thus, we do not need to explicitly know those normal velocities. This fact is important since if we had to model the absolute beam fields we would need a way to determine the "driving" normal velocities at the transmitting and receiving transducers in states (1) and (2), respectively. The normal velocities at the acoustic ports of these transducers are not easy quantities to determine experimentally, so it is fortunate that we do not need to know them to apply Eq. (11.28).

In state (2), the flaw is absent so that the stress and velocity fields appearing in that state in Eq. (11.28) are due to just the waves incident of the flaw surface. Those fields only require that we have an ultrasonic beam model in order to predict them. In state (1), however, the flaw is present, so that we must have both a beam model to predict the incident fields on the flaw in that state and a flaw scattering model that can predict the waves generated by the interaction of the incident waves with the flaw.

Equation (11.28) in a slightly different form was originally derived in 1979 by Bert Auld [11.1]. Because it is a very general result it has been frequently used as the basis for many ultrasonic modeling efforts world-wide. The main difference between Eq. (11.28) and Auld's original form is that Eq. (11.28) is an expression for the measured output voltage in an ultrasonic measurement system while Auld's result gave the measured flaw response in terms of a change of the fields present in a cable at the receiver. While this difference does not change the basic form of Eq. (11.28), it is an important difference when one wants to examine the elements in $s(\omega)$ as done in previous Chapters.

We can express Eq. (11.28) in a slightly different form that is also very useful. In both states (1) and (2), we assume the incident velocity field can be expressed as an incident plane wave modified by a spatially varying "amplitude" coefficient. Then we can write the incident velocity field in state (1) as (omitting the $\exp(-i\omega t)$ term):

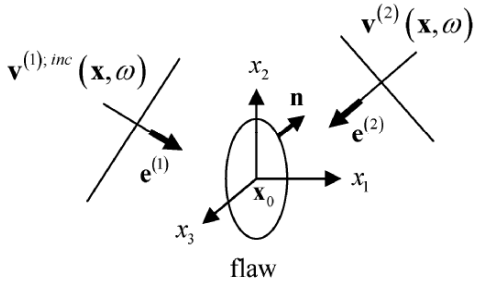

Fig. 11.6. The velocity fields incident on a flaw in states (1) and (2), respectively, which for small flaws can be treated locally as quasi-plane waves.

$$v_j^{(1);inc} = v_T^{(1)} \hat{V}^{(1)}(\mathbf{x},\omega) d_j^{(1)} \exp\left[ik_{\beta 2} e_n^{(1)} x_n \right] \tag{11.29}$$

and the incident velocity in state (2) as

$$v_j^{(2)} = v_R^{(2)} \hat{V}^{(2)}(\mathbf{x},\omega) d_j^{(2)} \exp\left[ik_{\alpha 2} e_n^{(2)} x_n \right] \tag{11.30}$$

where $\hat{V}^{(m)}(m=1,2)$ are the velocity field "amplitudes" (note that they are complex quantities) of the incident waves in states (1) and (2) normalized by the driving velocities on the faces of the transmitting transducers in those states. The $d_j^{(m)}(m=1,2)$ are polarizations of the incident waves in the two states, $k_{\alpha 2}$ and $k_{\beta 2}$ are the wave numbers for the incident waves in states (1) and (2) in the solid surrounding the flaw, respectively, and where α and β denote the incident wave type (P or S). The $e_n^{(m)}(m=1,2)$ terms are the components of the unit vectors in the direction of propagation for the incident waves in the two states. In Eqs. (11.29) and (11.30) the coordinates of the point $\mathbf{x}=(x_1,x_2,x_3)$ are measured from an origin located at point $\mathbf{x}_0$, which is a fixed point near the flaw, usually taken at the flaw "center" (see Fig. 11.6). Note that in state (1) the total velocity, $\mathbf{v}^{(1)}$ is given by $\mathbf{v}^{(1)} = \mathbf{v}^{(1);inc} + \mathbf{v}^{(1);scatt}$, where $\mathbf{v}^{(1);inc}$ is given by Eq. (11.29) and $\mathbf{v}^{(1);scatt}$ is the velocity field due to the waves scattered from the flaw, while in state (2), the total velocity field is only the incident field given by Eq. (11.30) since the flaw is absent in that state.

Using these quasi-plane wave forms in Eq. (11.28), we can write that equation in the form

$$V_R(\omega) = s(\omega)\left[\frac{4\pi\rho_2 c_{\alpha 2}}{-ik_{\alpha 2}Z_r^{T;a}}\right] \cdot \int_{S_f} \hat{V}^{(1)}(\mathbf{x},\omega)\hat{V}^{(2)}(\mathbf{x},\omega)\mathcal{A}(\mathbf{x},\omega)\exp\left[ik_{\alpha 2}e_n^{(2)}x_n\right]dS \tag{11.31}$$

with

$$\mathcal{A}(\mathbf{x},\omega) = \frac{1}{4\pi\rho_2 c_{\alpha 2}^2}\left[\tilde{\tau}_{ji}^{(1)}d_i^{(2)} + C_{ijkl}d_k^{(2)}\left(e_l^{(2)}/c_{\alpha 2}\right)\tilde{v}_i^{(1)}\right]n_j. \tag{11.32}$$

(no sum on α)

where $\rho_2, c_{\alpha 2}$ are the density and wave speed, respectively, for the material surrounding the flaw. The normalized velocity and stress terms $\tilde{v}_j^{(1)}, \tilde{\tau}_{ij}^{(1)}$ are defined as

$$\tilde{\tau}_{ij}^{(1)} = \frac{-i\omega\tau_{ij}^{(1)}}{v_T^{(1)}\hat{V}^{(1)}}$$
$$\tilde{v}_j^{(1)} = \frac{-i\omega v_j^{(1)}}{v_T^{(1)}\hat{V}^{(1)}}. \tag{11.33}$$

Physically, these normalized fields are the actual fields in state (1) normalized by an incident wave displacement amplitude term $U^{(1)}(\mathbf{x},\omega) = v_T^{(1)}\hat{V}^{(1)}(\mathbf{x},\omega)/(-i\omega)$.

Equation (11.31) begins to reveal some of the structure of the integral term that was not evident in Eq. (11.28). The $\hat{V}^{(1)}(\mathbf{x},\omega), \hat{V}^{(2)}(\mathbf{x},\omega)$ terms are quasi-plane wave incident field amplitudes at the flaw for states (1) and (2) due to the transmitting and receiving transducers radiating with a unit velocity on their surfaces. These terms can be modeled explicitly if one has a beam model such as the multi-Gaussian beam model of Chapter 9 and combines the beam model with terms that take into account the material attenuation present (see Appendix D). The remaining $\mathcal{A}$ term is closely related to the scattering properties of the flaw. If the displacement amplitude term $U^{(1)}$ was a constant or if it did not vary significantly over the surface of the flaw then the normalized velocity and stress fields in Eq. (11.32) would be those due to an incident plane wave of unit displacement amplitude on the flaw. But recall the component of the plane wave far-field scattering amplitude taken

in the $-\mathbf{d}^{(2)}$ direction, $A(\omega) \equiv \mathbf{A}^{\alpha;\beta}\left(\mathbf{e}^{(1)};\mathbf{e}^{(2)}\right)\cdot\left(-\mathbf{d}^{(2)}\right)$ is just given by (see Eqs. (10.6) and (10.7))

$$A(\omega) = \int_S \mathcal{A}(\mathbf{x},\omega)\exp\left(-ik_{\alpha 2}\mathbf{e}_s^{\alpha}\cdot\mathbf{x}\right)dS(\mathbf{x}_s). \tag{11.34}$$

[Note: to compare with the results in Chapter 10, in our current notation, $\mathbf{e}_i^{\beta} = \mathbf{e}^{(1)}$, $\mathbf{e}_s^{\alpha} = -\mathbf{e}^{(2)}$]. Thus, $\mathcal{A}$ contains the total fields on the surface of the flaw that in principle could be obtained by solving the flaw scattering problem and can be used to compute the far-field scattering amplitude component, $A(\omega)$. Of course, in Eq. (11.31) the far-field scattering amplitude component of Eq. (11.34) itself does not appear explicitly because of the beam variations contained in that equation but as we will see in the following section there are cases where the frequency spectrum of the received voltage is proportional directly to $A(\omega)$.

11.2 The Thompson-Gray Measurement Model

If we write the incident fields in states (1) and (2) as quasi-plane waves and if in addition we assume that the flaw is small enough so that the variations of the velocity field amplitudes $\hat{V}^{(m)}(m=1,2)$ are negligible over the surface of the flaw, we have

$$\begin{aligned} v_j^{(1);inc} &= v_T^{(1)}\hat{V}_0^{(1)}d_j^{(1)}\exp\left[ik_{\beta 2}e_n^{(1)}x_n\right] \\ v_j^{(2)} &= v_R^{(2)}\hat{V}_0^{(2)}d_j^{(2)}\exp\left[ik_{\alpha 2}e_n^{(2)}x_n\right], \end{aligned} \tag{11.35}$$

where $\hat{V}_0^{(m)}(\omega) \equiv \hat{V}^{(m)}(\mathbf{x}_0,\omega)\quad (m=1,2)$, i.e. the velocity field amplitudes are now constants evaluated at a fixed point, $\mathbf{x}_0$, in the vicinity of the flaw, which is usually taken at the "center" of the flaw (Fig. 11.6). We see from Eq. (11.35) that under this assumption these incident fields are now indeed treated as simply plane waves. Then Eq. (11.31) becomes

$$\begin{aligned} V_R(\omega) = s(\omega)\hat{V}_0^{(1)}\hat{V}_0^{(2)}&\left[\frac{4\pi\rho_2 c_{\alpha 2}}{-ik_{\alpha 2}Z_r^{T;a}}\right] \\ &\cdot\int_{S_f}\mathcal{A}(\mathbf{x},\omega)\exp\left[ik_{\alpha 2}e_n^{(2)}x_n\right]dS \end{aligned} \tag{11.36}$$

and the far-field scattering amplitude component does appear explicitly so we find, finally

$$V_R(\omega) = s(\omega)\hat{V}_0^{(1)}(\omega)\hat{V}_0^{(2)}(\omega)A(\omega)\left[\frac{4\pi\rho_2 c_{\alpha 2}}{-ik_{\alpha 2}Z_r^{T;a}}\right]. \tag{11.37}$$

A form similar to Eq. (11.37) was first obtained by Thompson and Gray in 1983 [11.2]. As we have seen, this Thompson-Gray measurement model is based on the general reciprocity-based measurement model (Eq. (11.28) and only two assumptions: 1) the incident waves can be expressed in a quasi-plane wave form, and 2) the flaw is small enough so that the amplitude of this quasi-plane wave does not vary significantly over the flaw surface [11.3]. With those two assumptions we obtain a modular measurement model where the flaw response, $A(\omega)$, is explicitly separated from all the other measurement system terms, including the system function, $s(\omega)$, and the normalized incident fields $\hat{V}_0^{(1)}, \hat{V}_0^{(2)}$ at the flaw from the transducers in states (1) and (2), respectively.

This separation of terms allows us to examine a ultrasonic measurement system in a variety of ways. For example, if the voltage response of an unknown flaw is measured and we also measure $s(\omega)$ and model the transducer beam fields $\hat{V}_0^{(1)}, \hat{V}_0^{(2)}$, we can write Eq. (11.37) in the form

$$V_R(\omega) = G(\omega)A(\omega), \tag{11.38}$$

where both $V_R(\omega)$ and $G(\omega)$ are known. In this case we can divide the measured voltage by the known G (using a Wiener filter) to obtain a measured flaw far-field scattering amplitude of the flaw. An example of this approach is given in Chapter 13. The flaw far-field scattering amplitude is related to the properties of the flaw only, so that we can use it in quantitative flaw characterization and sizing studies. Alternatively, we could model the beam fields and the scattering amplitude for an assumed flaw and measure the system function for a given measurement setup. In this case we could use Eq. (11.38) to predict the amplitude of the received signals from the known flaw directly. This information might be used, for instance, to optimize the transducer orientation during a scan so that the signals received from a given flaw are large. Engineering studies of these and other types can be done easily with the Thompson-Gray measurement model, so that it has been used for many practical industrial applications

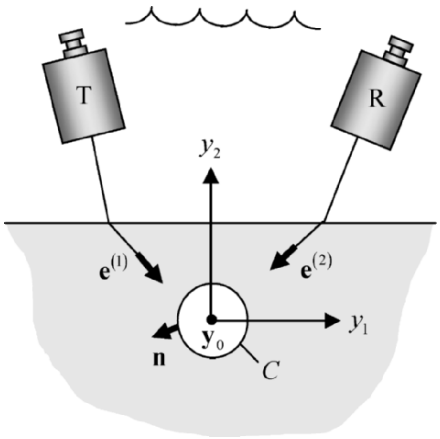

Fig. 11.7. A pitch-catch measurement of the scattering from a cylindrical reflector of length L where the axis of the cylinder is normal to planes of incidence for states (1) and (2).

(many examples are available in past volumes of Review of Progress in Quantitative Nondestructive Evaluation [11.4]).

11.3 A Measurement Model for Cylindrical Reflectors

The Thompson-Gray measurement model describes the ultrasonic response of a flaw where the variation of the incident fields can be neglected over the entire flaw surface. In some experiments cylindrical reflectors are used where the beam variations over the cross-section of the reflector may be neglected, but the variations over the length of the reflector are significant. An example is where a side-drilled hole is used as a reference reflector in a calibration block. Here, we will develop a measurement model suitable for these type of setups [11.5].

Consider the pitch-catch case shown in Fig. 11.7. We will assume that the reflector has a cylindrical geometry and is of length, L. We will also assume that the axis of the cylinder is normal to the planes of incidence of the incident waves in states (1) and (2), which are defined to be the planes that contain both the incident wave direction and the unit normal, $\mathbf{n}$, to the reflector. This is a reasonable assumption since in most setups where a 2-D reflector such as a side-drilled hole is used, the transducers are usually oriented so that this condition holds. With this

assumption it is reasonable to also assume that all the scattering occurs only from the cylindrical surface, i.e. the scattering from the ends of the reflector is neglected. For a side-drilled hole, for example, which is often drilled entirely through a reference calibration block, the length of the hole is generally larger than the axial extent of the interrogating transducer fields, so that this assumption is well satisfied.

Like the Thompson-Gray measurement model, we will also assume the incident fields in states (1) and (2) can be represented by the quasi-plane waves given by Eqs. (11.29) and (11.30). Thus, we can use as our starting point Eq. (11.31), which we write as:

$$V_R(\omega) = s(\omega)\left[\frac{4\pi\rho_2 c_{\alpha 2}}{-ik_{\alpha 2} Z_r^{T;a}}\right] \cdot \int_{S_c} \hat{V}^{(1)}(\mathbf{y},z,\omega)\hat{V}^{(2)}(\mathbf{y},z,\omega)\mathcal{A}\exp\left[ik_{\alpha 2} e_n^{(2)} x_n\right] dS, \tag{11.39}$$

where the integration is now over only the cylindrical surface, S_c, and the velocity field amplitudes over this surface are expressed as $\hat{V}^{(1)} = \hat{V}^{(1)}(\mathbf{y},z,\omega)$, $\hat{V}^{(2)} = \hat{V}^{(2)}(\mathbf{y},z,\omega)$ where $\mathbf{y} = (y_1, y_2)$ is a point in a plane normal to the cylinder axis and z is along the axis. If the cylinder is small enough to neglect the variations of these velocity fields over its cross-sectional area (but not neglecting these variations over its length) we let $\hat{V}^{(1)} = \hat{V}_0^{(1)}(z,\omega)$, $\hat{V}^{(2)} = \hat{V}_0^{(2)}(z,\omega)$, where

$$\begin{aligned} \hat{V}_0^{(1)}(z,\omega) &\equiv \hat{V}^{(1)}(\mathbf{y}_0,z,\omega) \\ \hat{V}_0^{(2)}(z,\omega) &\equiv \hat{V}^{(2)}(\mathbf{y}_0,z,\omega) \end{aligned} \tag{11.40}$$

and $\mathbf{y}_0$ is a fixed point, usually taken as the center of the reflector (Fig. 11.7). Then we can write Eq. (11.39) as

$$V_R(\omega) = s(\omega)\left[\frac{4\pi\rho_2 c_{\alpha 2}}{-ik_{\alpha 2} Z_r^{T;a}}\right] \cdot \int_C \int_L \hat{V}_0^{(1)}(z,\omega)\hat{V}_0^{(2)}(z,\omega)\mathcal{A}\exp\left[ik_{\alpha 2} e_n^{(2)} x_n\right] dc dz, \tag{11.41}$$

where the 2-D surface integration has been decomposed into a counter-clockwise line integral over the cross-section, C, and a 1-D integral over the length, L.

Now, consider the normalized fields appearing in the $\mathcal{A}$ term in Eq. (11.41). They are:

$$\tilde{v}_i^{(1)} = \frac{-i\omega v_i^{(1)}(\mathbf{y},z,\omega)}{\hat{V}_0^{(1)}(z,\omega)}$$
$$\tilde{\tau}_{ji}^{(1)} = \frac{-i\omega \tau_{ji}^{(1)}(\mathbf{y},z,\omega)}{\hat{V}_0^{(1)}(z,\omega)}. \tag{11.42}$$

We will also assume that these normalized fields are functions of **y** only, i.e. we assume the *z*-variations of the non-normalized fields are identical to those in the incident waves. In this case we then also have $\mathcal{A} = \mathcal{A}(\mathbf{y},\omega)$ only. This assumption is equivalent to breaking the cylindrical surface into small elements of length d*z* and at each *z* treating the scattering of each element as if it were a purely two-dimensional scattering process due to a plane wave whose displacement amplitude is given by $U^{(1)}(z,\omega) = v_T^{(1)}(\omega)\hat{V}_0^{(1)}(z,\omega)/(-i\omega)$. In Chapter 10, where the scattering amplitude for a side-drilled hole was calculated via the Kirchhoff approximation, this assumption was satisfied exactly. Here, we will make the assumption regardless of how the scattering problem for the cylinder is to be solved. With this assumption, then Eq. (11.41) becomes

$$V_R(\omega) = s(\omega)\left[\frac{4\pi\rho_2 c_{\alpha 2}}{-ik_{\alpha 2}Z_r^{T;a}}\right]\int_L \hat{V}_0^{(1)}(z,\omega)\hat{V}_0^{(2)}(z,\omega)\,dz$$
$$\cdot\int_C \mathcal{A}(\mathbf{y},\omega)\exp\left[ik_{\alpha 2}e_\lambda^{(2)}y_\lambda\right]dc(\mathbf{y}), \tag{11.43}$$

where the summation over the repeated λ subscript is taken over values (1,2) only.

But the far-field scattering amplitude of the cylindrical reflector is given by

$$A_{3D}(\omega) = L\int_C \mathcal{A}(\mathbf{y},\omega)\exp\left[ik_{\alpha 2}e_\lambda^{(2)}y_\lambda\right]dc(\mathbf{y}) \tag{11.44}$$

where we have used the "3D" label to emphasize that the reflector is still being treated as a three-dimensional scatterer even though under our assumptions the fields in Eq. (11.44) are all two-dimensional. With this definition, Eq. (11.43) can be reduced to

$$V_R(\omega) = s(\omega)\left[\int_L \hat{V}_0^{(1)}(z,\omega)\hat{V}_0^{(2)}(z,\omega)\,dz\right]\left[\frac{A_{3D}(\omega)}{L}\right]\left[\frac{4\pi\rho_2 c_{\alpha 2}}{-ik_{\alpha 2}Z_r^{T;a}}\right]. \tag{11.45}$$

Equation (11.45) is the measurement model for the cylindrical reflector that is the counterpart of Eq. (11.37) for the small three-dimensional flaw. In fact, if the incident velocity fields do not vary significantly also in the *z*-direction, we see that Eq. (11.45) simply reduces to Eq. (11.37).

Since under our assumptions the fields in Eq. (11.44) only depend on **y** and from our other assumptions we also have $n_3 = e_3^\alpha = d_3^\alpha = \tilde{v}_3^\alpha = 0$, Eq. (11.44) can be rewritten more explicitly as

$$A_{3D}(\omega) = \frac{L}{4\pi\rho_2 c_{\alpha 2}^2} \int_C \left[\tilde{\tau}_{\gamma\sigma}^{(1)} d_\sigma^{(2)} + C_{\sigma\gamma\nu\delta} d_\nu^{(2)} \left(e_\delta^{(2)} / c_{\alpha 2} \right) \tilde{v}_\sigma^{(1)} \right] \cdot n_\gamma \exp\left[ik_{\alpha 2} e_\lambda^{(2)} y_\lambda \right] dc, \quad \text{(no sum on } \alpha\text{)} \tag{11.46}$$

where all the Greek indices are summed over the values $(1,2)$ only (no sum on α). As shown in Chapter 10 this scattering amplitude component can be related to the corresponding far-field scattering amplitude component, $A_{2D}(\omega)$, in a purely two-dimensional scattering problem where both the incident fields and the geometry of the reflector are independent of the *z*-coordinate. That relationship was given as (see Eq. (10.63)):

$$A_{2D}(\omega) = \left(\frac{2\mathrm{i}\pi}{k_{\alpha 2}} \right)^{1/2} \frac{A_{3D}(\omega)}{L}. \tag{11.47}$$

Thus, we can express our ultrasonic measurement model for the cylinder either in terms of the three-dimensional far-field scattering amplitude of the reflector or its two-dimensional far-field scattering amplitude counterpart.

11.4 References

11.1 Auld BA (1979) General electromechanical reciprocity relations applied to the calculation of elastic wave scattering coefficients. Wave Motion 1: 3-10

11.2 Thompson RB, Gray TA (1983) A model relating ultrasonic scattering measurements through liquid-solid interfaces to unbounded medium scattering amplitudes. J. Acoust. Soc. Am. 74: 140-146

11.3 Schmerr LW (2004) Fundamentals of ultrasonic measurement models. In: Lee SS, Yoon DJ, Lee JH, Lee S (eds) Advances in nondestructive evaluation. Trans Tech Publications Ltd, USA pp 402-409

11.4 Thompson DO, Chimenti DE (eds) Review of progress in quantitative nondestructive evaluation. Plenum Press, New York, NY/ American Institute of Physics, Melville, NY. Past Volumes (1981-present)
11.5 Schmerr LW, Sedov A (2003) Modeling ultrasonic problems for the 2002 ultrasonic benchmark session. In: Thompson DO, Chimenti DE (eds) Review of progress in quantitative nondestructive evaluation 22B. American Institute of Physics, Melville, NY pp 1776-1783

11.5 Exercises

1. In Chapter 12, a multi-Gaussian beam model is used in conjunction with the Kirchhoff approximation to implement the Thompson-Gray measurement model (Eq. (11.37)) for the pulse-echo P-wave response of a spherical void, as shown in Fig. 11.8. However, one can also implement this measurement model directly using the results of Chapter 8 and Chapter 10. First note that for this pulse-echo setup Eq. (11.37) becomes

$$V_R(\omega) = s(\omega)\left[\hat{V}_0^{(1)}(\omega)\right]^2 A(\omega)\left[\frac{4}{-ik_{p2}a^2}\frac{\rho_2 c_{p2}}{\rho_1 c_{p1}}\right], \tag{11.48}$$

where a is the radius of the transducer, ρ_1, c_{p1} are the density and compressional wave speed of the fluid, ρ_2, c_{p2} are the density and wave speed of the solid, and $k_{p2} = \omega / c_{p2}$ is the wave number for compressional waves in the solid. The normalized on-axis velocity, $\hat{V}_0^{(1)}(\omega)$, can be obtained from Eq. (8.25) as

$$\hat{V}_0^{(1)}(\omega) = T_{12}^{P;P} \exp\left(-\alpha_{p1} z_1\right) \exp\left(ik_{p1} z_1 + ik_{p2} z_2\right)\left[1 - \exp\left(\frac{ik_{p1}a^2}{2\tilde{z}}\right)\right], \tag{11.49}$$

where $\tilde{z} = z_1 + c_{p2} z_2 / c_{p1}$ and $T_{12}^{p;p}$ is the plane wave transmission coefficient at normal incidence (see Eq. (D.36)):

$$T_{12}^{p;p} = \frac{2\rho_1 c_{p1}}{\rho_1 c_{p1} + \rho_2 c_{p2}}. \tag{11.50}$$

An attenuation factor has been included in Eq. (11.49) to account for the water attenuation. The attenuation of the solid (which is glass) has been neglected here. In implementing Eq. (11.49), omit the propagation terms

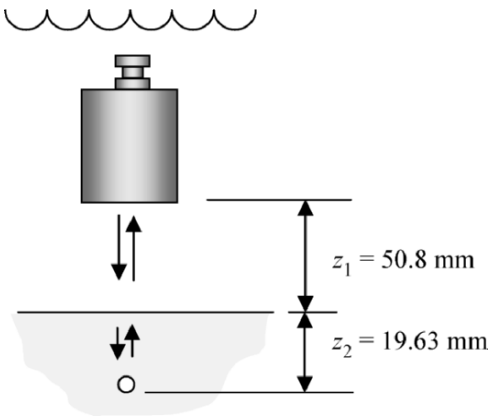

Fig. 11.8. Measurement of the pulse-echo P-wave response of an on-axis spherical pore.

$\exp\left(ik_{p1}z_1 + ik_{p2}z_2\right)$ as these only generate large phases that represent a time delay factor $\Delta t = z_1 / c_{p1} + z_2 / c_{p2}$ that can always be added in later, if necessary.

For the scattering amplitude term, $A(\omega)$, one can use the Kirchhoff approximation for the pulse-echo response of a void of radius *b* given by (Eq. (10.14)):

$$A(\omega) = \frac{-b}{2}\exp\left(-ik_{p2}b\right)\left[\exp\left(-ik_{p2}b\right) - \frac{\sin\left(k_{p2}b\right)}{k_{p2}b}\right]. \tag{11.51}$$

Write a MATLAB script that implements the Thompson-Gray measurement model of Eq. (11.48) for this on-axis spherical pore. The pertinent data for this problem are:

$a = 6.35\ mm$

$b = 0.34605\ mm$

$z_1 = 50.8\ mm$

$z_2 = 19.63\ mm$

$\rho_1 = 1.0\ gm/cm^3$

$c_{p1} = 1484\ m/\sec$

$\rho_2 = 2.2\ gm/cm^3$

$c_{p2} = 5969.4\ m/\sec$

$\alpha_{p1} = 0.02479 \times 10^{-3} f^2 \quad Np/mm\ (f\ in\ MHz)$

For the system function, $s(\omega)$, use the simulated MATLAB function system_f(f, amp, fc, bw) described in Appendix G. Take amp=0.08, fc = 5, bw = 4. These parameters simulate a system containing a broad band 5 MHz transducer. The frequency, f, in this function is measured in MHz.

The MATLAB script should calculate the received voltage from the void as a function of frequency, perform an inverse FFT to obtain the corresponding time-domain signal, and then plot this signal versus time. Verify that you results agree with Fig. 12.11 which is the solution of this same problem using a multi-Gaussian beam model instead of Eq. (11.49).